T_{cc}^+ and its partners

Chengrong Deng[1,2,*] and Shi-Lin Zhu[2,†]

[1]*School of Physical Science and Technology, Southwest University, Chongqing 400715, China*
[2]*School of Physics and Center of High Energy Physics, Peking University, Beijing 100871, China*

Inspired by the T_{cc}^+ signal discovered by the LHCb Collaboration, we systematically investigate the doubly heavy tetraquark states with the molecule configuration $[Q_1\bar{q}_2]_{\mathbf{1}_c}[Q_3\bar{q}_4]_{\mathbf{1}_c}$ ($Q = c$ and b, $q = u$, d, and s) in a nonrelativistic quark model. The model involves a color screening confinement potential, meson-exchange interactions, and one-gluon-exchange interactions. The state T_{cc}^+ with $IJ^P = 01^+$ is a very loosely bound deuteronlike state with a binding energy around 0.34 MeV and a huge size of 4.32 fm. Both the meson exchange force and the coupled channel effect play a pivotal role. Without the meson exchange force, there does not exist the T_{cc}^+ molecular state. In strong contrast, the QCD valence bond forms clearly in the T_{bb}^- system when we turn off the meson-exchange force, which is very similar to the hydrogen molecule in QED. Moreover, the T_{bb}^- becomes a heliumlike QCD-atom if we increase the bottom quark mass by a factor of three. Especially, the states T_{bb}^- with 01^+, T_{bc}^0 with 00^+ and 01^+, and the V-spin antisymmetric states T_{bbs}^- with $\frac{1}{2}1^+$, T_{bcs}^0 with $\frac{1}{2}0^+$ and $\frac{1}{2}1^+$ can form a compact, hydrogen moleculelike or deuteronlike bound state with different binding dynamics. The high-spin states T_{bc}^0 with 02^+ and T_{bcs}^0 with $\frac{1}{2}2^+$ can decay into D-wave $\bar{B}D$ and $\bar{B}_s D$ although they are below the thresholds $\bar{B}^* D^*$ and $\bar{B}_s^* D^*$, respectively. The isospin and V-spin symmetric states are unbound. We also calculate their magnetic moments and axial charges.

I. INTRODUCTION

The theoretical explorations on the possible stable doubly heavy tetraquark states were pioneered in the early 1980s [1]. These states were investigated with various formalisms such as the MIT bag model [2], constituent quark models [3,4], chiral perturbation theory [5], string model [6], lattice QCD [7], and QCD sum rule approach [8,9]. Although the state T_{bb}^- with 01^+ seems stable in various theoretical frameworks, its production turns out to be very challenging. The discovery of the doubly charmed baryon Ξ_{cc}^{++} by the LHCb Collaboration [10] has stimulated the enthusiasms on the doubly heavy tetraquark states [11–24].

Recently, the LHCb Collaboration discovered the doubly charmed state T_{cc}^+ with $IJ^P = 01^+$ by analyzing the $D^0 D^0 \pi^+$ invariant mass spectrum [25], which has a minimal quark configuration of $cc\bar{u}\bar{d}$. Its binding energy relative to the DD^* threshold and width are

*crdeng@swu.edu.cn
†zhusl@pku.edu.cn

$$E_b = -273 \pm 61 \pm 5^{+11}_{-14} \text{ keV},$$
$$\Gamma = 410 \pm 165 \pm 43^{+18}_{-38} \text{ keV}.$$

The LHCb Collaboration also released a more profound decay analysis, in which the unitarized Breit-Wigner profile was used [26]. Its binding energy and decay width were updated as

$$E_b = -361 \pm 40 \text{ keV}, \qquad \Gamma = 47.8 \pm 1.9 \text{ keV}.$$

The binding energy and decay width of the T_{cc}^+ signal match very well with the prediction of the DD^* molecular state [27,28]. The discovery of the $X(3872)$ [29] pioneered the observation of a family of hidden-charm and hidden-bottom tetraquark and pentaquark states in the past decades. Similarly, the discovery of the T_{cc}^+ shall open a new gate for a family of the T_{cc}^+-like doubly heavy tetraquark, pentaquark and hexaquark states.

The discovery of the state T_{cc}^+ has inspired a large amount of investigations on its properties and structure within the different theoretical frameworks [28,30–46]. Many T_{cc}^+-like doubly heavy tetraquark candidates were proposed, such as the states T_{cc}' [36], T_{bb}^- [43], T_{ccs}^+ [47,48], T_{bc}^0 [49], T_{bcs}^0 [49], S-wave $D_1 D_1$, $D_1 D_2^*$ and $D_2^* D_2^*$ states [50], doubly charmed P_{cc} and triply charmed H_{ccc} states [51–53].

In this work, we will analyze the underlying dynamics in the formation of the loosely bound T_{cc}^+ state very carefully. We will exhaust the most promising partners of the T_{cc}^+ and compare the different binding mechanisms in the T_{cc}^+ and T_{bb}^- systems.

This paper is organized as follows. After the Introduction, the details of the quark model are given in Sec. II. The construction of the wave functions of the doubly heavy tetraquark states with the molecule configuration is shown in Sec. III. The numerical results and discussions of the stable doubly heavy tetraquark states are presented in the following sections. The last section is a brief summary.

II. QUARK MODEL

The underlying theory of strong interaction is quantum chromodynamics (QCD). At the hadronic scale, QCD is highly nonperturbative due to the complicated infrared behavior of the non-Abelian $SU(3)$ gauge group. At present it is still impossible to derive the hadron spectrum analytically from the QCD Lagrangian. The QCD-inspired constituent quark model remains a powerful tool in obtaining physical insight for the complicated strong interaction systems although the connection between the light current quarks in QCD and the light constituent quarks in the quark model is not established clearly.

The constituent quark model was formulated under the assumption that the hadrons are color singlet nonrelativistic bound states of constituent quarks with phenomenological effective masses and various effective interactions. The model Hamiltonian used here can be written as

$$H_n = \sum_{i=1}^{n} \left(m_i + \frac{\mathbf{p}_i^2}{2m_i} \right) - T_c + \sum_{i>j}^{n} V_{ij},$$

$$V_{ij} = V_{ij}^{\text{oge}} + V_{ij}^{obe} + V_{ij}^{\sigma} + V_{ij}^{\text{con}},$$

where m_i and $\mathbf{p}_i$ are the mass and momentum of the ith quark or antiquark, respectively. T_c is the center-of-mass kinetic energy of the states and should be deducted. V_{ij}^{oge}, V_{ij}^{obe}, V_{ij}^{σ}, and V_{ij}^{con} are the one-gluon-exchange interaction, one-boson-exchange interaction (π, K and η), σ-meson exchange interaction and color confinement potential between the particles i and j, respectively.

The origin of the constituent quark mass can be traced back to the spontaneous breaking of $SU(3)_L \otimes SU(3)_R$ chiral symmetry and consequently constituent quarks should interact through the exchange of Goldstone bosons [54]. Chiral symmetry breaking suggests dividing quarks into two different sectors: light quarks (u, d and s) where the chiral symmetry is spontaneously broken and heavy quarks (c and b) where the symmetry is explicitly broken. The meson exchange interactions only occur in the light quark sector. The central parts of the interactions

originating from chiral symmetry breaking can be resumed as follows [55],

$$V_{ij}^{obe} = V_{ij}^{\pi} \sum_{k=1}^{3} \mathbf{F}_i^k \mathbf{F}_j^k + V_{ij}^{K} \sum_{k=4}^{7} \mathbf{F}_i^k \mathbf{F}_j^k$$
$$+ V_{ij}^{\eta} (\mathbf{F}_i^8 \mathbf{F}_j^8 \cos\theta_P - \sin\theta_P),$$

$$V_{ij}^{\chi} = \frac{g_{ch}^2}{4\pi} \frac{m_{\chi}^3}{12 m_i m_j} \frac{\Lambda_{\chi}^2}{\Lambda_{\chi}^2 - m_{\chi}^2} \boldsymbol{\sigma}_i \cdot \boldsymbol{\sigma}_j$$
$$\times \left(Y(m_{\chi} r_{ij}) - \frac{\Lambda_{\chi}^3}{m_{\chi}^3} Y(\Lambda_{\chi} r_{ij}) \right), \quad \chi = \pi, K \text{ and } \eta$$

$$V_{ij}^{\sigma} = -\frac{g_{ch}^2}{4\pi} \frac{\Lambda_{\sigma}^2 m_{\sigma}}{\Lambda_{\sigma}^2 - m_{\sigma}^2} \left(Y(m_{\sigma} r_{ij}) - \frac{\Lambda_{\sigma}}{m_{\sigma}} Y(\Lambda_{\sigma} r_{ij}) \right).$$

The noncentral parts, tensor force and spin-orbit coupling, are not given because we are only interested in the S-wave states here. The function $Y(x) = \frac{e^{-x}}{x}$, $\mathbf{F}_i$ and $\boldsymbol{\sigma}_i$ are the flavor $SU(3)$ Gell-Mann matrices and spin $SU(2)$ Pauli matrices, respectively. r_{ij} is the distance between the particles i and j. The mass parameters m_{π}, m_K and m_{η} take their experimental values. The cutoff parameters Λs and the mixing angle θ_P take the values from Ref. [55]. The mass parameter m_{σ} can be determined through the PCAC relation $m_{\sigma}^2 \approx m_{\pi}^2 + 4 m_{u,d}^2$ [56]. The chiral coupling constant g_{ch} can be obtained from the πNN coupling constant through

$$\frac{g_{ch}^2}{4\pi} = \left(\frac{3}{5} \right)^2 \frac{g_{\pi NN}^2}{4\pi} \frac{m_{u,d}^2}{m_N^2}.$$

Besides the chiral symmetry breaking, there also exists the one-gluon-exchange (OGE) potential. From the non-relativistic reduction of the OGE diagram in QCD for the pointlike quarks, one gets

$$V_{ij}^{\text{oge}} = \frac{\alpha_s}{4} \boldsymbol{\lambda}_i^c \cdot \boldsymbol{\lambda}_j^c \left(\frac{1}{r_{ij}} - \frac{2\pi\delta(\mathbf{r}_{ij})\boldsymbol{\sigma}_i \cdot \boldsymbol{\sigma}_j}{3 m_i m_j} \right),$$

$\boldsymbol{\lambda}_i$ is the color $SU(3)$ Gell-Mann matrices. The Dirac $\delta(\mathbf{r}_{ij})$ function, where $\mathbf{r}_{ij} = \mathbf{r}_i - \mathbf{r}_j$, arises from the interaction between pointlike quarks and collapses when not treated perturbatively [57]. Therefore, the $\delta(\mathbf{r}_{ij})$ function is regularized in the form [55]

$$\delta(\mathbf{r}_{ij}) \rightarrow \frac{1}{4\pi r_{ij} r_0^2(\mu_{ij})} e^{-r_{ij}/r_0(\mu_{ij})},$$

where $r_0(\mu_{ij}) = \hat{r}_0/\mu_{ij}$, $\hat{r}_0$ is an adjustable model parameter and μ_{ij} is the reduced mass of two interacting particles i and j. This regularization is justified based on the finite size of the constituent quarks and should be flavor dependent [58].

The quark-gluon coupling constant α_s in the perturbative QCD reads [59]

$$\alpha_s(\mu^2) = \frac{1}{\beta_0 \ln \frac{\mu^2}{\Lambda^2}},$$

In the present work, we use an effective scale-dependent form given by

$$\alpha_s(\mu_{ij}^2) = \frac{\alpha_0}{\ln \frac{\mu_{ij}^2}{\Lambda_0^2}},$$

Λ_0 and α_0 are adjustable model parameters determined by fitting the ground state meson spectrum.

Finally, any model imitating QCD should incorporate the nonperturbative color confinement effect. We adopt the phenomenological color screening confinement potential,

$$V_{ij}^{con} = -a_c \lambda_i^c \cdot \lambda_j^c f(r_{ij})$$

$$f(r_{ij}) = \begin{cases} r_{ij}^2 & \text{if } i, j \text{ occur in the same meson,} \\ \frac{1-e^{-\mu_c r_{ij}^2}}{\mu_c} & \text{if } i, j \text{ occur in different mesons.} \end{cases}$$

It is different from the form of confinement potential used in recent investigations on the doubly heavy tetraquark states [20,21]. The adjustable parameter a_c is determined by fitting the ground state meson spectrum. The color screening parameter $\mu_c = 1.0 \text{ fm}^{-2}$ is taken from Ref. [60]. The color screening confinement potential can automatically match the quadratic one in the short distance region ($\mu_c r^2 \ll 1$). When two mesons are separated to large distances, the confinement potential can guarantee that the energy of the tetraquark system evolves into the sum of the two-meson internal energy calculated by the model Hamiltonian. In the intermediate range region, the hybrid confinement can give a different picture from that given by a single form confinement. Such type of the color screening confinement potential comes from the quark delocalization and color screening model [60], which can describe the nuclear intermediate range attraction and reproduce the $N - N$ scattering data and the properties of the deuteron. Meanwhile, the model can avoid the spurious van de Walls color force between two color singlets arising from the direct extension of the single-hadron Hamiltonian to the multiquark states [60]. The model has been widely applied to investigate the properties of the baryon-baryon and baryon-meson interactions [61].

III. WAVE FUNCTIONS OF THE DOUBLY HEAVY TETRAQUARK STATES

Our previous systematical investigation on the doubly heavy tetraquark states suggested that the states $[Q_1 Q_3][\bar{q}_2 \bar{q}_4]$ can establish deep compact bound states in the quark models [11], which is obviously contradictive with the properties of the state T_{cc}^+ reported by the LHCb Collaboration [25,26].

The research on the states $[Q_1 \bar{q}_2][Q_3 \bar{q}_4]$ indicated that their main color component is the molecule state $[Q_1 \bar{q}_2]_{1_c}[Q_3 \bar{q}_4]_{1_c}$ [20]. Furthermore, recent study on the states $[c\bar{u}][c\bar{d}]$ and $[b\bar{u}][b\bar{d}]$ shown that the hidden color components $[[c\bar{u}]_{8_c}[c\bar{d}]_{8_c}]_{1_c}$ and $[[b\bar{u}]_{8_c}[b\bar{d}]_{8_c}]_{1_c}$ can be negligible if all possible color singlet components were taken into account [62]. The influence of the hidden color components on the numerical results is very insignificant even if the hidden color configurations are included. In order to reduce the heavy computational workload, we therefore omit the hidden color configuration $[[Q_1 \bar{q}_2]_{8_c}[Q_3 \bar{q}_4]_{8_c}]_{1_c}$ in the present work.

Within the framework of the molecule configuration $[c_1 \bar{u}_2]_{1_c}[c_3 \bar{d}_4]_{1_c}$, the trial wave function of the T_{cc}^+ state with $IJ^P = 01^+$ can be constructed as a sum of the following direct products of color ψ_c, isospin η_i, spin χ_s and spatial ϕ terms

$$\Phi_{IJ}^{T_{cc}^+} = \sum_\alpha \mathcal{A} \Big\{ [[\phi_{l_a m_a}^G(\mathbf{r})\chi_{s_a}]_{J_a M_{J_a}}^{[c_1 \bar{u}_2]} [\phi_{l_b m_b}^G(\mathbf{R})\chi_{s_b}]_{J_b M_{J_b}}^{[c_3 \bar{d}_4]} $$
$$\times \phi_{l_c m_c}^G(\boldsymbol{\rho})]_{JM_J}^{T_{cc}^+} [\eta_{i_a}^{[c_1 \bar{u}_2]} \eta_{i_b}^{[c_3 \bar{d}_4]}]_I^{T_{cc}^+} [\psi_{c_a}^{[c_1 \bar{u}_2]} \psi_{c_b}^{[c_3 \bar{d}_4]}]_C^{T_{cc}^+} \Big\}.$$

Here we assume the magnetic components $M_I = I$ and $M_J = J$. The subscripts a and b represent the subclusters $[c_1 \bar{u}_2]$ and $[c_3 \bar{d}_4]$, respectively. $\mathcal{A}$ is the antisymmetrization operator and equal to $1 - P_{13} - P_{24} + P_{13} P_{24}$ because of the Fermi-Dirac statistic of the identical particles, where P_{ij} is the permutation operator on the particles i and j. The summing index α stands for all possible flavor-spin-color-spatial intermediate quantum numbers.

The relative spatial coordinates $\mathbf{r}$, $\mathbf{R}$ and $\boldsymbol{\rho}$ are defined as

$$\mathbf{r} = \mathbf{r}_1 - \mathbf{r}_2, \qquad \mathbf{R} = \mathbf{r}_3 - \mathbf{r}_4,$$
$$\boldsymbol{\rho} = \frac{m_1 \mathbf{r}_1 + m_2 \mathbf{r}_2}{m_1 + m_2} - \frac{m_3 \mathbf{r}_3 + m_4 \mathbf{r}_4}{m_3 + m_4}.$$

The corresponding angular excitations of three relative motions are, respectively, l_a, l_b, and l_c. The parity of the state T_{cc}^+ can therefore be expressed in terms of the relative orbital angular momenta associated with the Jacobi coordinates as $P = (-1)^{l_a + l_b + l_c}$. It is worth mentioning that this set of coordinate is only a possible choice of many coordinates and however most propitious to describe the correlation of two mesons. In order to obtain a reliable solution of few-body problem, a high precision numerical method is indispensable. The Gaussian expansion method (GEM) [63] has been proven to be very powerful to solve the few-body problem. Brink *et al.* first applied the GEM for studying heavy tetraquarks states [4]. We also use the GEM to study doubly heavy tetraquark systems in the present work. According to the GEM, the relative motion wave function can be written as

$$\phi_{lm}^{G}(\mathbf{x}) = \sum_{n=1}^{n_{\max}} c_n N_{nl} x^l e^{-\nu_n x^2} Y_{lm}(\hat{\mathbf{x}})$$

Gaussian size parameters are taken as geometric progression

$$\nu_n = \frac{1}{r_n^2}, \qquad r_n = r_1 a^{n-1}, \qquad a = \left(\frac{r_{n_{\max}}}{r_1}\right)^{\frac{1}{n_{\max}-1}}. \qquad (1)$$

r_1 and $r_{\max}$ are the minimum and maximum of the size, respectively. $n_{\max}$ is the number of the Gaussian wave function. More details about the GEM can be found in Ref. [63]. In the present work, we expand the wave function $\phi_{l_a m_a}^{G}(\mathbf{r})$ ($\phi_{l_b m_b}^{G}(\mathbf{R})$) with $n_{\max}$ ($n'_{\max}$) Gaussian functions with the different width ranging from 0.1 fm to 2.0 fm because the size of the mesons is less than 1 fm. We expand the wave function $\phi_{l_c m_c}^{G}(\boldsymbol{\rho})$ with $n''_{\max}$ Gaussian functions with the different width ranging from 0.1 fm to 5.0 fm because the size of meson-meson molecule is about several fms. In this way, the total number of the trial wave function N_{base} is equal to $n_{csf} \times n_{\max} \times n'_{\max} \times n''_{\max}$, where n_{csf}, the number of the color-spin-flavor wave function, will be given later. N_{base} should be increased gradually by increasing $n_{\max}$, $n'_{\max}$ and $n''_{\max}$ until the convergent numerical results are obtained. In addition, a large width Gaussian function $\phi_{l_c m_c}^{G}(\boldsymbol{\rho})$ ($\rho = |\boldsymbol{\rho}| \to \infty$) should be introduced to guarantee a fast convergence of numerical results when a bound state does not exist.

Taking all degrees of freedom of identical particles, the Pauli principle must be satisfied by imposing a restriction on the quantum numbers of the mesons $c_1 \bar{u}_2$ and $c_3 \bar{d}_4$. The quantum numbers must satisfy the relation $s_a + s_b - S + i_a + i_b - I + l_c =$ even when $s_a = s_b$ because the present boson system should satisfy the boson-Einstein statistic. According to the restriction, the S-wave ($l_c = 0$) states with 00^+ and 02^+ do not exist. The wave function of the S-wave state $[c_1 \bar{u}_2][\bar{c}_3 \bar{d}_4]$ with 01^+ has two possible channels,

$$[DD^*]_- = \frac{1}{\sqrt{2}}(D^{0*}D^+ - D^+ D^*),$$

$$[D^*D^*]_- = \frac{1}{\sqrt{2}}(D^{*0}D^{*+} - D^{*+}D^{*0}),$$

In the channel $[D^*D^*]_-$, the spins of the mesons D^{*0} and D^{*+} couple into the total angular momentum J. Similarly, the wave function of the state $[c_1 \bar{u}_2][\bar{c}_3 \bar{d}_4]$ with 10^+ also has two possible channels,

$$[DD]_+ = \frac{1}{\sqrt{2}}(D^0 D^+ + D^+ D^0),$$

$$[D^*D^*]_+ = \frac{1}{\sqrt{2}}(D^{*0}D^{*+} + D^{*+}D^{*0}).$$

The wave functions of the states $[c_1 \bar{u}_2][\bar{c}_3 \bar{d}_4]$ with 11^+ and 12^+ can be written as

$$[DD^*]_+ = \frac{1}{\sqrt{2}}(D^0 D^{*+} + D^{*+} D^0),$$

$$[D^*D^*]_+ = \frac{1}{\sqrt{2}}(D^{*0}D^{*+} + D^{*+}D^{*0}).$$

Analogically, there may exist the partners of the T_{cc}^+ state with the configurations of $[b_1 \bar{u}_2][b_3 \bar{d}_4]$ and $[b_1 \bar{u}_2][c_3 \bar{d}_4]$, denoted as T_{bb}^- and T_{bc}^0. We can obtain the wave functions of the S-wave state T_{bb}^- by solely making a replacement of c with b in those of the state T_{cc}^+. In the case of the state T_{bc}^0, the wave functions of the states with 00^+ and 10^+ read

$$[\bar{B}D]_{\pm} = \frac{1}{\sqrt{2}}(B^- D^+ \pm \bar{B}^0 D^0),$$

$$[\bar{B}^*D^*]_{\pm} = \frac{1}{\sqrt{2}}(B^{-*}D^{+*} \pm \bar{B}^{0*}D^{0*}).$$

The signs $+$ and $-$ stand for the cases of the isospin symmetry ($I = 1$) and antisymmetry ($I = 0$), respectively. The same notations hold for the other states with $I = 1$ and $I = 0$. The wave functions of the states $[b_1 \bar{u}_2][c_3 \bar{d}_4]$ with 01^+ and 11^+ have the following three possible channels,

$$[\bar{B}D^*]_{\pm} = \frac{1}{\sqrt{2}}(B^- D^{+*} \pm \bar{B}^0 D^{0*}),$$

$$[\bar{B}^*D]_{\pm} = \frac{1}{\sqrt{2}}(B^{-*}D^+ \pm \bar{B}^{0*}D^0),$$

$$[\bar{B}^*D^*]_{\pm} = \frac{1}{\sqrt{2}}(B^{-*}D^{+*} \pm \bar{B}^{0*}D^{0*}).$$

The wave function of the states with 02^+ and 12^+ has the following one possible channel,

$$[\bar{B}^*D^*]_{\pm} = \frac{1}{\sqrt{2}}(B^{-*}D^{+*} \pm \bar{B}^{0*}D^{0*}).$$

We denote the strange partners of the T_{cc}^+ state with the configurations $[b_1 \bar{u}_2][b_3 \bar{s}_4]$, $[c_1 \bar{u}_2][c_3 \bar{s}_4]$, and $[b_1 \bar{u}_2][c_3 \bar{s}_4]$ as the T_{bbs}^-, T_{ccs}^+, and T_{bcs}^0, respectively. We can obtain their wave functions by replacing $\bar{d}$ with $\bar{s}$ in those of the states T_{bb}^-, T_{cc}^+, and T_{bc}^0 because I-spin (isospin) and V-spin are equivalent. The wave functions of the states $[b_1 \bar{s}_2][b_3 \bar{s}_4]$, $[c_1 \bar{s}_2][c_3 \bar{s}_4]$, and $[b_1 \bar{s}_2][c_3 \bar{s}_4]$, denoted as the T_{bbss}^0, T_{ccss}^{++}, and T_{bcss}^+, are similar to those of the states T_{bb}^-, T_{cc}^+, and T_{bc}^0 with $I = 1$ because they have the same flavor symmetry.

IV. STRUCTURE OF THE T_{cc}^+ STATE WITH 01^+

We reproduce the mass spectrum of the ordinary mesons to determine model parameters as in Ref. [11]. We collect the results of the heavy-light mesons in Table I.

TABLE I. The $Q\bar{q}$ meson spectrum in the model where the mass unit is in MeV and $\langle r^2\rangle^{\frac{1}{2}}$ unit in fm.

State	D	D^*	D_s	D_s^*	$\bar{B}$	$\bar{B}^*$	$\bar{B}_s$	$\bar{B}_s^*$
Cal.	1867	2002	1972	2140	5259	5301	5377	5430
PDG	1869	2007	1968	2112	5280	5325	5366	5416
$\langle r^2\rangle^{\frac{1}{2}}$	0.68	0.82	0.52	0.69	0.73	0.77	0.57	0.62

In the following, we move on to the investigation of the T_{cc}^+ with 01^+ and its partners. In order to obtain the lowest states with positive parity, we assume that the three relative motions are in S-wave, namely $l_a = l_b = l_c = 0$. We can obtain the eigenvalue and eigenvector by solving the four-body Schrödinger equation

$$(H_4 - E_4)\Phi_{IJ}^{T_{cc}^+} = 0$$

with the Rayleigh-Ritz variational principle. We define the binding energy E_b of the doubly heavy tetraquark states as

$$E_b = E_4 - \lim_{\rho\to\infty} E_4(\rho)$$

to identify whether or not the tetraquark states are stable against the strong interactions, where $\lim_{\rho\to\infty} E_4(\rho)$ is the lowest theoretical threshold of the two mesons which can couple into the same quantum numbers with those of the tetraquark states. Such a subtraction procedure can greatly reduce the influence of the inaccurate model parameters and meson spectra on the binding energies. If $E_b \geq 0$, the tetraquark systems can fall apart into two mesons via the strong interactions. If $E_b < 0$, the strong decay into two mesons is forbidden and therefore the decay can only occur via either the weak or electromagnetic interaction.

We can obtain the convergent numerical results of the state T_{cc}^+ with 01^+ with more than 4600 bases in the spin-color-flavor-orbital space, which are presented in Table II. It can be seen from Table II that the binding energy $E_b = -0.342$ MeV predicted by the model is highly consistent with the data given by the LHCb Collaboration. Note that no adjustable parameter is introduced to match the experimental data in our calculation. Neither of the single

$[DD^*]_-$ and $[D^*D^*]_-$ channel alone can form a bound state in the model. The stable T_{cc}^+ state arises from the coupling of these two channels. The dominant component of the state T_{cc}^+ is the DD^* channel. Therefore, the coupled channel effect plays a critical role in the formation of the state T_{cc}^+ under the assumption of the molecule picture.

The spatial configuration of the state T_{cc}^+ can be ascertained by the sizes of the two subclusters D (D^*) and D^* and their relative distance, which can be approximately described by the rms $\langle \mathbf{r}^2\rangle^{\frac{1}{2}}$, $\langle \mathbf{R}^2\rangle^{\frac{1}{2}}$ and $\langle \boldsymbol{\rho}^2\rangle^{\frac{1}{2}}$ determined by the eigenvectors, respectively. The sizes $\langle \mathbf{r}^2\rangle^{\frac{1}{2}}$ and $\langle \mathbf{R}^2\rangle^{\frac{1}{2}}$ are approximately those of the individual meson listed in Table I, which is far less than the distance between two subclusters $\langle \boldsymbol{\rho}^2\rangle^{\frac{1}{2}} = 4.32$ fm. In other words, the two subclusters are far away from each other. Therefore, the T_{cc}^+ state is a loosely bound deuteronlike state consisted of D and D^*, see Fig. 1. The extracted T_{cc}^+ size 4.32 fm confirms the prediction of a huge size 4.46 fm with a binding energy 0.47 MeV in Ref. [27], which also agrees with the spatial configuration given by the LHCb Collaboration according to the characteristic size calculated from the binding energy [26].

In order to illustrate the mechanism of the formation of the T_{cc}^+ state, we calculate and decompose the contribution to the binding energy E_b from various parts of the Hamiltonian E_b^i in the following four cases: (a) with meson exchange and color screening effect, $\mu_c = 1$; (b) with meson exchange while without color screening effect, $\mu_c = 0$; (c) without meson exchange while with color screening effect, $\mu_c = 1$; (d) without meson exchange and color screening effect, $\mu_c = 0$. In the present model, the meson exchange and color screening effect only occur between two subclusters in the T_{cc}^+ state and do not affect the corresponding threshold. We present the numerical results in Table III, in which ΔE_k is the kinetic energy difference between the tetraquark system and its corresponding threshold. In addition, the binding energy of each single channel and its ratio in the eigenvector are also given in Table III.

The hybrid color screening confinement potential generally gives bigger binding energies than single type of one, see the cases (a) and (b) or (c) and (d) in the states T_{bc}^0, T_{bbs}^-,

TABLE II. The stability of numerical results, E_b unit in MeV, r, r', r'' and rms unit in fm.

$\phi_{00}^G(\mathbf{r})$			$\phi_{00}^G(\mathbf{R})$			$\phi_{00}^G(\boldsymbol{\rho})$			N_{base}	$[DD^*]_-$ E_b, Ratio	$[D^*D^*]_-$ E_b, Ratio	Mixing E_b	Rms		
r_1	r_{max}	n_{max}	r_1'	r_{max}'	n_{max}'	r_1''	r_{max}''	n_{max}''					$\langle \mathbf{r}^2\rangle^{\frac{1}{2}}$	$\langle \mathbf{R}^2\rangle^{\frac{1}{2}}$	$\langle \boldsymbol{\rho}^2\rangle^{\frac{1}{2}}$
0.1	2.0	7	0.1	2.0	7	0.1	5.0	20	1960	0.000, 99.6%	0.000, 0.4%	−0.330	0.75	0.75	4.41
0.1	2.0	8	0.1	2.0	8	0.1	5.0	21	2688	0.000, 99.6%	0.000, 0.4%	−0.353	0.75	0.75	4.23
0.1	2.0	9	0.1	2.0	9	0.1	5.0	22	3654	0.000, 99.6%	0.000, 0.4%	−0.344	0.75	0.75	4.30
0.1	2.0	10	0.1	2.0	10	0.1	5.0	23	4600	0.000, 99.6%	0.000, 0.4%	−0.342	0.75	0.75	4.32
0.1	2.0	11	0.1	2.0	11	0.1	5.0	24	5808	0.000, 99.6%	0.000, 0.4%	−0.342	0.75	0.75	4.32
0.1	2.0	12	0.1	2.0	12	0.1	5.0	25	7200	0.000, 99.6%	0.000, 0.4%	−0.342	0.75	0.75	4.32
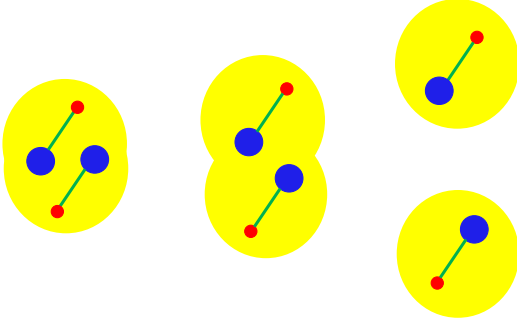
FIG. 1. The spatial configuration, left: compact state; middle: hydrogen moleculelike state; right: deuteronlike state, big blue ball and small red ball represent Q and $\bar{q}$, respectively. A large yellow ball represents a subcluster.

and T_{bcs}^0. However, the order is reversed in the cases (a) and (b) of the states T_{cc}^+ and T_{bb}^- because of their stronger meson exchange interaction relative to the confinement potential.

From the cases (c) and (d) in Table III, the bound state T_{cc}^+ vanishes if we turn off the meson exchange interactions in the model. In other words, the long-range π and intermediate-range σ meson exchange force play a pivotal role in the formation of the loosely bound T_{cc}^+ state.

We further compare the cases (a) and (b) to illustrate the very delicate competition between the kinetic energy and the attraction from various sources in the Hamiltonian. The main factor hindering the formation of the D (D^*) and D^* subclusters into the bound state is the relative kinetic

TABLE III. The properties of the state T_{cc}^+ and its partners predicted by the model, E_b unit in MeV and rms unit in fm. ΔE_k is the kinetic energy difference between the tetraquark system and its corresponding threshold. Four cases: (a) with meson exchange and color screening effect; (b) with meson exchange while without color screening effect; (c) without meson exchange while with color screening effect; (d) without meson exchange and color screening effect. The "−" denotes that the single channel is unbound.

State case	IJ^P μ_c	Channel E_b, ratio			Mixing E_b	$\langle\mathbf{r}^2\rangle^{\frac{1}{2}}$	$\langle\mathbf{R}^2\rangle^{\frac{1}{2}}$	$\langle\boldsymbol{\rho}^2\rangle^{\frac{1}{2}}$	V^σ	V^π	V^K	V^η	V^{con}	V^{oge}	ΔE_k
T_{cc}^+	01^+	$[\bar{D}\bar{D}^*]_-$	$[\bar{D}^*\bar{D}^*]_-$												
(a)	1.0	−, 99.6%	−, 0.4%		−0.34	0.75	0.75	4.32	−2.68	−2.19	0.00	0.17	−1.00	−4.29	9.65
(b)	0.0	−, 98.8%	−, 1.2%		−0.86	0.76	0.76	2.94	−3.72	−5.41	0.00	0.49	−1.87	−7.88	17.51
(c)	1.0	−, 100%	−, 0.0%		−										
(d)	0.0	−, 100%	−, 0.0%		−										
T_{bb}^-	01^+	$[\bar{B}\bar{B}^*]_-$	$[\bar{B}^*\bar{B}^*]_-$												
(a)	1.0	**−11.2**, 80.6%	**−9.8**, 19.4%		−28.6	0.79	0.79	0.59	−15.8	−57.9	0.0	6.6	−16.7	−108.3	163.5
(b)	0.0	**−10.0**, 62.4%	**−9.0**, 37.6%		−43.8	0.84	0.84	0.46	−17.0	−76.0	0.0	8.6	−21.8	−111.7	174.1
(c)	1.0	**−0.3**, 84.7%	**−0.2**, 15.3%		−10.0	0.72	0.72	1.04					−2.5	3.4	−10.9
(d)	0.0	−, 94.8%	−, 5.2%		−3.9	0.73	0.73	1.65					−1.4	−10.1	7.6
T_{bc}^0	00^+	$[\bar{B}D]_-$	$[\bar{B}^*D^*]_-$												
(a)	1.0	**−9.0**, 98.6%	−, 1.4%		−12.9	0.71	0.66	1.09	−9.9	−1.4	0.0	0.2	−5.1	−28.6	31.9
(b)	0.0	**−5.7**, 98.6%	**−3.5**, 1.4%		−10.5	0.71	0.67	1.14	−9.9	−5.0	0.0	0.6	−4.9	−34.4	43.1
(c)	1.0	**−4.8**, 99.6%	−, 0.4%		−6.5	0.71	0.66	1.37					−2.3	−9.2	5.0
(d)	0.0	**−2.1**, 99.8%	−, 0.2%		−3.0	0.71	0.66	1.82					−1.2	−13.1	11.4
T_{bc}^0	01^+	$[\bar{B}D^*]_-$	$[\bar{B}^*D]_-$	$[\bar{B}^*D^*]_-$											
(a)	1.0	**−6.5**, 0.5%	**−7.7**, 98.7%	**−3.0**, 0.8%	−10.5	0.75	0.66	1.20	−8.4	0.6	0.0	0.1	−4.0	−15.7	16.9
(b)	0.0	**−2.7**, 0.1%	**−4.4**, 97.2%	**−1.3**, 2.7%	−7.6	0.77	0.68	1.30	−8.1	−3.6	0.0	0.4	−3.8	−21.7	29.2
(c)	1.0	**−3.5**, 0.8%	**−3.9**, 98.7%	−, 0.5%	−6.3	0.75	0.66	1.40					−2.1	−3.2	−1.1
(d)	0.0	**−0.6**, 0.2%	**−1.4**, 99.6%	−, 0.2%	−2.2	0.76	0.67	2.07					−0.9	−8.0	6.7
T_{bc}^0	02^+		$[\bar{B}^*D^*]_-$												
(a)	1.0		**−12.0**, 100%		−12.0	0.74	0.79	1.28	−6.4	7.3	0.0	−0.5	−2.8	0.4	−10.0
(b)	0.0		**−3.6**, 100%		−3.6	0.75	0.79	1.88	−4.3	4.5	0.0	−0.3	−0.8	−3.7	0.9
(c)	1.0		**−12.4**, 100%		−12.4	0.74	0.79	1.25					−3.7	−0.6	−8.0
(d)	0.0		**−3.6**, 100%		−3.6	0.75	0.79	1.83					−1.3	−4.6	2.0
T_{bbs}^-	$\frac{1}{2}1^+$	$[\bar{B}\bar{B}_s^*]_-$	$[\bar{B}^*\bar{B}_s^*]_-$												
(a)	1.0	**−4.8**, 91.1%	**−4.2**, 8.9%		−11.8	0.66	0.66	0.94	−11.2	0.0	0.3	0.1	−3.5	−6.1	8.6
(b)	0.0	**−3.8**, 96.0%	**−3.4**, 4.0%		−9.0	0.68	0.68	0.97	−11.4	0.0	−2.3	−0.4	−4.0	−21.4	30.4
(c)	1.0	−, 90.1%	−, 9.9%		−3.3	0.67	0.67	1.30					−0.6	5.4	−8.1
(d)	0.0	−, 97.6%	−, 2.4%		−0.5	0.68	0.68	2.74					−0.2	−1.6	1.3

(Table continued)

TABLE III. *(Continued)*

State case	IJ^P μ_c	Channel E_b, ratio			Mixing E_b	Rms $\langle \mathbf{r}^2 \rangle^{\frac{1}{2}}$	$\langle \mathbf{R}^2 \rangle^{\frac{1}{2}}$	$\langle \boldsymbol{\rho}^2 \rangle^{\frac{1}{2}}$	E_b^i V^σ	V^π	V^K	V^η	V^{con}	V^{oge}	ΔE_k
T_{bcs}^0	$\frac{1}{2}0^+$	$[\bar{B}_s D]_-$	$[B^*D^*]_-$												
(a)	1.0	**−7.4**, 99.6%	−, 0.4%		−9.2	0.64	0.60	1.13	−10.3	0.0	0.8	0.1	−3.0	−15.6	18.8
(b)	0.0	**−5.1**, 99.6%	−, 0.4%		−6.7	0.64	0.60	1.25	−9.5	0.0	0.4	0.1	−2.4	−20.2	24.9
(c)	1.0	**−1.1**, 99.8%	−, 0.2%		−1.6	0.65	0.60	2.00					0.6	−4.3	2.1
(d)	0.0	0.1, 99.9%	−, 0.1%		−0.4	0.65	0.61	3.33					−0.2	−4.2	4.0
T_{bcs}^0	$\frac{1}{2}1^+$	$[\bar{B}_s D^*]_-$	$[\bar{B}_s^* D]_-$	$[\bar{B}_s^* D^*]_-$											
(a)	1.0	**−4.9**, 0.5%	**−6.1**, 99.1%	−, 0.4%	−8.0	0.69	0.60	1.21	−8.9	0.0	1.0	0.2	−2.5	−6.7	8.9
(b)	0.0	**−2.3**, 0.2%	**−3.8**, 99.6%	−, 0.2%	−5.0	0.69	0.60	1.42	−7.8	0.0	0.6	0.1	−1.8	−11.9	15.8
(c)	1.0	**−0.5**, 0.4%	**−0.7**, 99.4%	−, 0.2%	−1.8	0.70	0.60	2.04					−0.5	−2.1	0.9
(d)	0.0	−, 0.1%	−, 99.8%	−, 0.1%	−0.2	0.70	0.60	5.53					−0.1	−2.2	2.1
T_{bcs}^0	$\frac{1}{2}2^+$		$[\bar{B}_s^* D^*]_-$												
(a)	1.0		**−12.2**, 100%		−12.2	0.68	0.73	1.15	−7.9	0.0	1.7	0.3	−3.2	−0.2	−2.8
(b)	0.0		**−5.4**, 100%		−5.4	0.68	0.73	1.48	−6.2	0.0	1.2	0.2	−1.7	−4.6	5.7
(c)	1.0		**−6.6**, 100%		−6.6	0.69	0.75	1.36					−1.6	1.3	−6.4
(d)	0.0		**−1.4**, 100%		−1.4	0.69	0.75	2.33					−0.4	−1.9	1.0

energy between two subclusters in the cases (a) and (b). The interactions V^σ, V^π, V^{con} and V^{oge} provide precious attractions. Without the color screening effect, the confinement and one-gluon-exchange color forces between the two subclusters become stronger, which pull them closer to each other. Now all the meson exchange contributions become larger in magnitude. Especially, the one-pion-exchange force is extremely sensitive to the distance and its contribution to the binding energy increases to −5.41 MeV. In contrast, the kinetic energy difference ΔE_k increases to 17.51 MeV in the case (b). The binding energy $E_b = -0.86$ MeV in the case (b) is also in good agreement with the experimental data. Therefore, the T_{cc}^+ state always emerges as a loosely bound state so long as there exists the meson exchange interactions.

V. ISOSPIN ANTISYMMETRIC T_{bb}^- STATES

A. Compact T_{bb}^-

Both of the $[\bar{B}\bar{B}^*]_-$ and $[\bar{B}^*\bar{B}^*]_-$ channels with 01^+ can form a bound state alone and their binding energies are about 10 MeV in the cases (a) and (b). After coupling the two channels, the state T_{bb}^- becomes a rather deeply bound state with $E_b = -28.6$ MeV and −43.8 MeV, respectively, which are much less that of the bound state T_{bb}^- with diquark-antidiquark structure $[bb][\bar{u}\,\bar{d}]$ because of their different color configurations [11,22]. Our present results are very close to the latest lattice QCD predictions in the range of 20–40 MeV [64]. However, the earlier lattice QCD results indicated that these states were over 100 MeV below the $\bar{B}\bar{B}^*$ threshold [65,66]. The strong attraction comes

from the interactions V^σ, V^π, V^{con} and V^{oge} in the model. Especially, the contributions from the V^{oge} and V^π are quite large, which is due to the rather compact size of the T_{bb}^- system.

The main component of the T_{bb}^- is the $[\bar{B}\bar{B}^*]_-$. The two subclusters $\bar{B}$ ($\bar{B}^*$) and $\bar{B}^*$ become obscure and overlap with each other severely because the sizes of the subclusters $\langle \mathbf{r}^2 \rangle^{\frac{1}{2}}$ and $\langle \mathbf{R}^2 \rangle^{\frac{1}{2}}$ are bigger than the relative distance $\langle \boldsymbol{\rho}^2 \rangle^{\frac{1}{2}}$ between the two subclusters, see Fig. 1. The large b quark mass allows the two subclusters to get as close as possible. The T_{bb}^- state with 01^+ looks like a compact tetraquark state if there exists the meson exchanges interaction. If so, the T_{bb}^- state may not be a pure meson-meson molecule state. Instead, it may be a mixture of the meson-meson molecule and other hidden color states. The specific ratio between two components needs further study. Such a qualitative feature is supported by the lattice QCD computations [64,67], in which the ratio of the meson-meson molecule component is about 60%.

B. Deuteronlike T_{bb}^-

If we remove the meson exchange interactions and color screening effect from the model and focus on the case (d) in Table III, the T_{bb}^- state with 01^+ becomes a shallow bound state with $E_b = -3.9$ MeV and $\langle \boldsymbol{\rho}^2 \rangle^{\frac{1}{2}} = 1.65$ fm, where the attraction mainly comes from the residual one-gluon-exchange potential V^{oge}. The two subclusters are separated too far away to overlap each other because the sum of the sizes of the subclusters $\langle \mathbf{r}^2 \rangle^{\frac{1}{2}}$ and $\langle \mathbf{R}^2 \rangle^{\frac{1}{2}}$ is less than their relative distance $\langle \boldsymbol{\rho}^2 \rangle^{\frac{1}{2}}$. Quarks are only allowed to move in

the isolated subclusters. Therefore, the T_{bb}^- state with 01^+ looks like a loosely bound deuteronlike molecular state in the case (d), see Fig. 1.

C. Hydrogen moleculelike T_{bb}^-

If we consider the color screening effect in the case (c) in Table III, the T_{bb}^- state with 01^+ forms a bound state with $E_b = -10$ MeV and $\langle \rho^2 \rangle^{\frac{1}{2}} = 1.04$ fm, where the attraction mainly arises from the decreasing of the kinetic energy. This novel mechanism is completely different from those in the other three cases, where the V^{oge} and (or) the meson exchange interactions provide a strong attraction while the kinetic energy prevents the two subclusters to form a bound state.

The two subclusters overlap with each other extremely in the cases (a) and (b) while they do not overlap at all in the case (d). Now in the case (c), the two subclusters $\bar{B}$ ($\bar{B}^*$) and $\bar{B}^*$ moderately overlap with each other, see Fig. 1. Such an appropriate spatial overlapping greatly enlarges the phase space of the light quarks $\bar{q}_2$ and $\bar{q}_4$ and allows them to roam into the opposite subcluster freely, which helps to lower the kinetic energy of the T_{bb}^- system. This is the realization of the uncertainty principle.

The delocalization of the light quarks in the state T_{bb}^- is extremely similar to the valence bond in the hydrogen molecule, where the electron pair is shared by two protons. Therefore, the T_{bb}^- state with 01^+ is very similar to the hydrogen molecule state, which is formed by the delocalization of the light quarks with the color screening effect in the case (c) in the present model. The idea of the QCD valence bond was proposed and investigated in Ref. [8] in 2013 and discussed extensively in the review [68]. Recently, Maiani *et al.* discussed the hydrogen molecule-like T_{bb}^- state when the $[bb]$ pair is in color **6** [69]. Richard *et al.* also studied the hydrogen moleculelike doubly heavy tetraquark states [70].

D. Heliumlike QCD atom in the limit of a large m_Q

In order to reveal the dependence of the three configurations on the heavy quark mass, we increase the bottom quark mass from m_b to m_Q with the mass ratio $\frac{m_Q}{m_b}$ and calculate the binding energy E_b and the average distances. We present numerical results in Table IV. One can see that the binding energy E_b in the three configurations is very sensitive to the mass ratio. The deeply bound state appears in the limit of a large m_Q. The large heavy quark mass permits them to get as close as possible (see $\langle \mathbf{r}_{QQ}^2 \rangle^{\frac{1}{2}}$ in Table IV), therefore their attractive Coulomb interaction becomes dominant. The binding energies of the B (deuteronlike) and C (hydrogenlike) configurations are close to each other. Their absolute values are smaller than that of the A (compact) configuration because of the extra attraction from the meson exchange interactions.

TABLE IV. Variation of the configurations with the mass ratio $\frac{m_Q}{m_b}$. $\langle \mathbf{r}_{QQ}^2 \rangle^{\frac{1}{2}}$ and $\langle \mathbf{r}_{\bar{u}\bar{d}}^2 \rangle^{\frac{1}{2}}$ are the average distance between Q and Q and $\bar{u}$ and $\bar{d}$, respectively. Others have their original meanings.

Configuration	$\frac{m_Q}{m_b}$	E_b	$\langle \mathbf{r}_{QQ}^2 \rangle^{\frac{1}{2}}$	$\langle \mathbf{r}_{\bar{u}\bar{d}}^2 \rangle^{\frac{1}{2}}$	$\langle \rho^2 \rangle^{\frac{1}{2}}$	$\langle \mathbf{r}^2 \rangle^{\frac{1}{2}}$	$\langle \mathbf{R}^2 \rangle^{\frac{1}{2}}$
A	1	−28.6	0.62	1.13	0.59	0.79	0.79
	2	−93.5	0.26	0.97	0.26	0.81	0.81
	3	−140.6	0.19	0.95	0.19	0.81	0.81
	4	−190.0	0.16	0.94	0.16	0.81	0.81
	5	−226.0	0.14	0.93	0.14	0.81	0.81
B	1	−3.9	1.73	1.95	1.65	0.73	0.73
	2	−19.2	0.65	1.19	0.62	0.80	0.80
	3	−58.1	0.22	1.06	0.22	0.91	0.91
	4	−97.1	0.17	1.06	0.17	0.91	0.91
	5	−131.4	0.15	1.06	0.15	0.91	0.91
C	1	−10.0	1.10	1.48	1.04	0.72	0.72
	2	−25.9	0.79	1.29	0.77	0.78	0.78
	3	−37.7	0.43	1.10	0.42	0.82	0.82
	4	−75.6	0.17	1.02	0.17	0.88	0.88
	5	−110.3	0.15	1.02	0.15	0.88	0.88

If we increase the ratio $\frac{m_Q}{m_b}$, the sizes of the subclusters are convergent in each configuration, see $\langle \mathbf{r}^2 \rangle^{\frac{1}{2}}$ and $\langle \mathbf{R}^2 \rangle^{\frac{1}{2}}$ in Table IV. However, the distance between two heavy quarks $\langle \mathbf{r}_{QQ}^2 \rangle^{\frac{1}{2}}$ decreases gradually till they shrink into a tiny and compact core eventually. The two subclusters overlap completely. The three configurations will degenerate into a single one. Its size can be approximately described by either the $\langle \mathbf{r}^2 \rangle^{\frac{1}{2}}$ or $\langle \mathbf{R}^2 \rangle^{\frac{1}{2}}$. The QQ-core contributes to the vast majority of the binding energy of the doubly heavy tetraquark states. The light quarks $\bar{u}$ and $\bar{d}$ move around the QQ-core. Their relative distance $\langle \mathbf{r}_{\bar{u}\bar{d}}^2 \rangle^{\frac{1}{2}}$ is about 1 fm. In summary, the doubly heavy tetraquark states look like a heliumlike QCD-atom in the limit of a large heavy quark mass.

VI. OTHER PARTNER STATES OF THE T_{cc}^+

A. Isospin antisymmetric states T_{bc}^0

The state T_{bc}^0 with 00^+ can form a shallow bound state with the E_b of several or a dozen MeV in the four cases, in which the dominant component is the channel $\bar{B}D$. Our conclusion is very close to that of other model calculations [27,71]. In the cases (a) and (b), the overlapping between two subclusters is very obvious so that the state looks like a compact state because of the strong attraction coming from the V^{oge} and V^σ. Turning off the meson exchange interactions, the T_{bc}^0 state with 00^+ becomes a loosely bound state in the cases (c) and (d) while a hydrogen moleculelike state does not appear.

The nonidentity of the b and c quark in the T_{bc}^0 state with 01^+ enlarges the Hilbert space comparing with the T_{bb}^- case with 01^+. Now we have to consider three coupling channels.

From Table III, the 01^+ state has a binding energy of several MeV in the four cases, which is slightly lower than the lattice QCD results in the range of 20–40 MeV below the $\bar{B}^*D$ threshold [49]. The dominant component of the state is the $\bar{B}^*D$ channel, which is supported by other model predictions [27,71]. The T_{bc}^0 state with 01^+ is a shallower bound state than the T_{bb}^- with 01^+ because of the lighter charm quark mass and thus larger kinetic energy. Moreover, the overlapping between the two subclusters, binding energy and the delocalization effect of the light quarks become weaker. However, the physical picture such as the emergence of the compact state, hydrogen moleculelike state or deuteronlike state in four cases in the T_{bc}^0 system resembles that of the T_{bb}^- state with 01^+.

The mass of the T_{bc}^0 state with 02^+ is about 12 MeV lower than the $\bar{B}^*\bar{D}^*$ threshold due to its small kinetic energy E_k in the model, see the cases (a) and (c) in Table III. This state can form a hydrogenlike state similar to the T_{bb}^- with 01^+ due to the delocalization of the light quarks induced by the color screening effect in the confinement. In the cases (b) and (d), the state has a binding energy of 3.6 MeV relative to the $\bar{B}^*\bar{D}^*$ threshold, which is a deuteronlike state because the two subclusters are separated well apart. The T_{bc}^0 state with 02^+ is not stable although it is below the $\bar{B}^*\bar{D}^*$ threshold because it can decay into the modes $\bar{B}D$, $\bar{B}D\pi$, $\bar{B}^*D\gamma$, $\bar{B}D^*\gamma$, $\bar{B}D\gamma\gamma$ etc. However, the state should be very narrow.

B. V-spin antisymmetric states T_{bbs}^- and T_{bcs}^0

The corresponding SU(2) groups of the I-spin, and the so-called V-spin and U-spin are three subgroups of the flavor SU(3) group. Therefore, the V-spin antisymmetric T_{bbs}^- with $\frac{1}{2}1^+$ and the state T_{bb}^- with 01^+ should share the same symmetry in their wave functions so that their behaviors should be analogous from the perspective of quark models. Similar arguments hold for the V-spin antisymmetric state T_{bcs}^0 and the state T_{bc}^0 with $I = 0$.

From Table III, the V-spin antisymmetric state T_{bbs}^- with $\frac{1}{2}1^+$ is a shallow bound state with a binding energy about 10 MeV relative to the threshold $\bar{B}\bar{B}_s^*$, where the attraction mainly comes from the V^σ in the cases (a) and (b). Our results agree with those in Ref. [27] but are less than the latest lattice QCD results about 80 MeV [72]. Similar to the state T_{bb}^- with 01^+, the state T_{bbs}^- with $\frac{1}{2}1^+$ can also form a compact state in the cases (a) and (b), which should therefore be a compound of color singlet and hidden color states. The lattice result indicated that the meson-meson percentage is about 84% while the hidden color percentage is about 16% [72]. In the case (c), the state T_{bbs}^- is a hydrogen moleculelike bound state because of the delocalization of the light quark $\bar{u}$ and $\bar{s}$ induced by the color screen effect. In the case (d), the state T_{bbs}^- forms a deuteronlike state because of removing the meson

exchange interaction and color screening effect from the model.

Both of the V-spin antisymmetric states T_{bcs}^0 with $\frac{1}{2}0^+$ and $\frac{1}{2}1^+$ appear a bound state in the model, which is qualitatively consistent with the conclusions in Refs. [27,49,73]. In the cases (a) and (b), the two states are shallow bound states with a binding energy of several MeV because of the V^σ. The two subclusters have a slight or even no overlapping. In the cases (c) and (d), the two states are very loosely bound without the meson exchange interactions. The two states are deuteronlike states because the subclusters are completely separated from each other. The hydrogen moleculelike configuration appearing in the state T_{bbs}^- with 01^+ vanishes in the T_{bcs}^0 states with $\frac{1}{2}0^+$ and $\frac{1}{2}1^+$.

The state T_{bcs}^0 with $\frac{1}{2}2^+$ is lower than the corresponding threshold $\bar{B}_s^*\bar{D}^*$ in the model. Similar to the state T_{bc}^0 with 02^+, the state T_{bcs}^0 with $\frac{1}{2}2^+$ is also a hydrogen moleculelike bound state because of the delocalization of light quarks in the cases (a) and (c). Removing the color screen effect from the model, the state T_{bcs}^0 with $\frac{1}{2}2^+$ becomes a deuteronlike bound state in the cases (b) and (d). The state is not stable and can decay into $\bar{B}_sD$, $\bar{B}_sD\pi$, $\bar{B}_sD^*\gamma$, $\bar{B}_s^*D\gamma$, $\bar{B}_sD\gamma\gamma$.

C. Other unstable states

All of the isospin symmetric states T_{cc}^+, T_{bb}^-, T_{bc}^0, T_{ccss}^{++}, T_{bbss}^0, and T_{bcss}^+ cannot form bound states because the interactions cannot provide enough attraction in the model. Other model studies on the states T_{bc}^0 and T_{ccss}^{++} also suggest that the isospin symmetric states are unbound and unstable [27,71,74,75]. The lattice QCD investigations on the isospin symmetric states T_{cc}^+, T_{bb}^-, T_{bc}^0, T_{ccss}^{++}, T_{bbss}^0 and T_{bcss}^+ indicated that no clear signal of any level below their respective thresholds can be found [66]. Similarly, the V-spin symmetric states T_{ccs}^+, T_{bbs}^-, and T_{bcs}^0 cannot form stable bound states in the model. The V-spin antisymmetric state T_{ccs}^+ with $\frac{1}{2}1^+$, the strange partner of the state T_{cc}^+ with 01^+, could be a stable bound state in some theoretical frameworks [27,47,48]. However, the state is not stable in the present model. The situation may change if the mixing of $S - D$ wave is taken into account in the model, which is left for future work.

VII. MAGNETIC MOMENTS AND AXIAL CHARGES

The magnetic moments of hadrons encode useful information about the distributions of the charge and magnetization inside the hadrons, which help us to understand their geometric configurations. Ignoring the contributions from the quark orbital angular momentum, the operator for the magnetic moment of the doubly heavy tetraquark system is given simply by

TABLE V.   Magnetic moment μ_m unit in μ_N and axial charge g_A unit in g_V in the four cases.

State	T_{cc}^+	T_{bb}^-	T_{bc}^0			T_{bbs}^-	T_{bcs}^0		
IJ^P	01^+	01^+	00^+	01^+	02^+	$\frac{1}{2}1^+$	$\frac{1}{2}0^+$	$\frac{1}{2}1^+$	$\frac{1}{2}2^+$
μ_m^a	0.18	0.64	0.00	0.66	0.79	1.37	0.00	0.98	1.29
μ_m^b	0.13	0.49	0.00	0.59	0.79	1.29	0.00	0.94	1.29
μ_m^c	-	0.97	0.00	0.72	0.79	1.40	0.00	0.95	1.29
μ_m^d	-	0.98	0.00	0.67	0.79	1.37	0.00	1.13	1.29
g_A^a	0.00	0.00	0.00	0.00	0.00	0.81	0.00	1.13	2.18
g_A^b	0.00	0.00	0.00	0.00	0.00	0.74	0.00	1.09	2.13
g_A^c	0.00	0.00	0.00	0.00	0.00	0.83	0.00	1.09	2.15
g_A^d	0.00	0.00	0.00	0.00	0.00	0.79	0.00	1.03	2.08

$$\hat{\mu}_m = \sum_{i=1}^{4} \frac{\hat{Q}_i}{2m_i} \hat{\sigma}_i^z,$$

where $\hat{Q}_i$ is the electric charge operator of the ith quark and the σ_i^z is the z-component of Pauli matrix. We can obtain the magnetic moments of the doubly heavy tetraquark states below their corresponding threshold by directly calculating the matrix element

$$\mu_m = \langle \Phi_{IJ} | \hat{\mu}_m | \Phi_{IJ} \rangle,$$

where Φ_{IJ} is the eigenvector of those states.

From Table V, the spin and magnetic momentums of the states T_{bc}^0 with 00^+ and T_{bcs}^+ with $\frac{1}{2}0^+$ vanish. The magnetic momentums of the other states depend on their spatial configurations except for the two high spin states. The magnetic momentum of the T_{cc}^+ state with 01^+ is about 0.18 μ_N and 0.13 μ_N in the cases (a) and (b), respectively. The magnetic momentum of the T_{cc}^+ state with 01^+ was also studied using the light-cone QCD sum rule formalism [76]. Its value was roughly 0.66 μ_N and 0.43 μ_N for the compact diquark-antidiquark and molecule pictures, respectively in Ref. [76].

The axial charge g_A is an important quantity for the understanding of both the electroweak and strong interactions. The nonrelativistic leading order axial charge operator for a pointlike Dirac constituent quark is given by the Gamov-Teller operator $\hat{\sigma}^z \hat{\tau}^z$ [77], where τ^z is the isospin operator. Then the axial charge operator for the doubly heavy tetraquark states is given by

$$\hat{g}_A = \sum_{i=1}^{4} \hat{\tau}_i^z \hat{\sigma}_i^z.$$

In this way, we can achieve the axial charge g_A of the states by directly calculating the matrix element

$$g_A = \langle \Phi_{IJ} | \hat{g}_A | \Phi_{IJ} \rangle,$$

which are presented in Table V. The axial charges of the states T_{cc}^+, T_{bb}^-, and T_{bc}^0 are zero because their isospin magnetic components are zero while that of T_{bcs}^0 with $\frac{1}{2}0^+$ is zero because its spin magnetic component is zero. The axial charges of the other states also depend on their spatial configurations but do not change dramatically in the four cases.

VIII. SUMMARY

In the present work, we have performed a systematical investigation of the doubly heavy tetraquark states with the molecule configuration within the framework of the non-relativistic quark model with the help of the Gaussian expansion method. The model includes the color screening confinement potential, meson-exchange interactions and one-gluon-exchange interactions. Besides the tetraquark spectrum and their spatial configurations, we have also calculated the magnetic moments and axial charges of the statable doubly heavy tetraquark states.

We discuss various dynamical effects in the formation of the stable bound states against the strong interactions extensively. We decompose the attractions from various sources and illustrate the very delicate competition between the kinetic energy and attractive potentials in the formation of three kinds of different bound states: the compact, deuteronlike or hydrogen moleculelike states.

The dominant component of the recently discovered T_{cc}^+ state by the LHCb Collaboration is the DD^* component, which cannot form a bound state alone in the model. The coupled channel effect between the $[DD^*]_-$ and $[D^*D^*]_-$ channels plays a critical role in the formation of the T_{cc}^+ under the assumption of meson-meson picture. The long-range π and intermediate-range σ exchange interactions also play a pivotal role. Without the meson exchange force, the T_{cc}^+ states does not exist. With the model parameters extracted from the ordinary meson spectrum and without introducing any new parameters in the present calculation, we extracted the binding energy of the T_{cc}^+ to be 0.34 MeV, which agrees with LHCb's measurement very well. With a huge size around 4.32 fm, the T_{cc}^+ state is a loosely bound deuteronlike state.

There is a broad theoretical consensus that the tendency to form doubly heavy tetraquark bound states is proportional to the mass ratio $\frac{m_Q}{m_q}$. In the limit of large masses of the heavy quarks the corresponding ground state should be deeply bound. Such a qualitative picture is strengthened by our numerical results. The existence of the shallow bound state T_{cc}^+ implies that there should exist many stable doubly heavy tetraquark states.

Our investigations indicate that the I-spin antisymmetric states T_{bb}^- with 01^+, T_{bc}^0 with 00^+ and 01^+, the V-spin antisymmetric states T_{bbs}^- with $\frac{1}{2}1^+$, T_{bcs}^0 with $\frac{1}{2}0^+$ and $\frac{1}{2}1^+$ can form a compact, hydrogen moleculelike, or deuteron-like bound state depending on different binding dynamics.

The compact spatial size of the T_{bb}^- may require the introduction of the hidden-color configuration from the very beginning, which is the topic of our future work.

The high-spin states T_{bc}^0 with 02^+ and T_{bcs}^0 with $\frac{1}{2}2^+$ can decay into D-wave $\bar{B}D$ and $\bar{B}_sD$ through the strong interactions although they are below the thresholds $\bar{B}^*D^*$ and $\bar{B}_s^*D^*$, respectively. The I-spin or V-spin symmetric states, T_{cc}^+, T_{bc}^0, T_{bb}^-, T_{bcs}^0, T_{bbs}^-, T_{ccss}^{++}, T_{bcss}^+, and T_{bbss}^0, are unbound in the model prediction. The state T_{ccs}^+ is also not bound in the model no matter its V-spin is symmetric or antisymmetric, which may be due to the omission of the $S-D$ wave mixing in the present work.

The discovery of the T_{cc}^+ state opened a new window for hadron physics. More theoretical and experimental efforts are called for in order to understand its underlying structure and nonperturbative QCD dynamics in this region. We sincerely hope that some of the doubly heavy tetraquark candidates may be searched for at LHCb and BelleII in the near future.

ACKNOWLEDGMENTS

[1] J. P. Ader, J. M. Richard, and P. Taxil, Phys. Rev. D **25**, 2370 (1982); J. L. Ballot and J. M. Richard, Phys. Lett. **123B**, 449 (1983).

[2] J. Carlson, L. Heller, and J. A. Tjon, Phys. Rev. D **37**, 744 (1988).

[3] S. Zouzou, B. Silvestre-Brac, C. Gignoux, and J. Richard, Z. Phys. C **30**, 457 (1986); B. Silvestre-Brac and C. Semay, Z. Phys. C **59**, 457 (1993); J. Vijande, A. Valcarce, and K. Tsushima, Phys. Rev. D **74**, 054018 (2006); Y. C. Yang, C. R. Deng, J. L. Ping, and T. Goldman, Phys. Rev. D **80**, 114023 (2009).

[4] D. M. Brink and Fl. M. Stancu, Phys. Rev. D **57**, 6778 (1998);

[5] A. V. Manohar and M. B. Wise, Nucl. Phys. **B399**, 17 (1993).

[6] J. Vijande, A. Valcarce, and J.-M. Richard, Phys. Rev. D **76**, 114013 (2007); C. Ay, J. M. Richard, and J. H. Rubinstein, Phys. Lett. B **674**, 227 (2009).

[7] P. Bicudo and M. Wagner, Phys. Rev. D **87**, 114511 (2013); Y. Ikeda, B. Charron, S. Aoki, T. Doi, T. Hatsuda, T. Inoue, N. Ishii, K. Murano, H. Nemura, and K. Sasaki, Phys. Lett. B **729**, 85 (2014).

[8] M. L. Du, W. Chen, X. L. Chen, and S. L. Zhu, Phys. Rev. D **87**, 014003 (2013).

[9] W. Chen, T. G. Steele, and S. L. Zhu, Phys. Rev. D **89**, 054037 (2014).

[10] R. Aaij et al. (LHCb Collaboration), Phys. Rev. Lett. **119**, 112001 (2017).

[11] C. R. Deng, H. Chen, and J. L. Ping, Eur. Phys. J. A **56**, 9 (2020).

[12] M. Karliner and J. L. Rosner, Phys. Rev. Lett. **119**, 202001 (2017).

[13] E. J. Eichten and C. Quigg, Phys. Rev. Lett. **119**, 202002 (2017).

[14] A. Francis, R. J. Hudspith, R. Lewis, and K. Maltman, Phys. Rev. Lett. **118**, 142001 (2017).

[15] P. Bicudo, J. Scheunert, and M. Wagner, Phys. Rev. D **95**, 034502 (2017).

[16] A. Czarnecki, B. Leng, and M. B. Voloshin, Phys. Lett. B **778**, 233 (2018).

[17] S. S. Agaev, K. Azizi, B. Barsbay, and H. Sundu, Phys. Rev. D **99**, 033002 (2019).

[18] A. Francis, R. J. Hudspith, R. Lewis, and K. Maltman, Phys. Rev. D **99**, 054505 (2019).

[19] Q. F. Lü, D. Y. Chen, and Y. B. Dong, Phys. Rev. D **102**, 034012 (2020).

[20] G. Yang, J. Ping, and J. Segovia, Phys. Rev. D **101**, 014001 (2020).

[21] Y. Tan, W. C. Lu, and J. L. Ping, Eur. Phys. J. Plus **135**, 716 (2020).

[22] Q. Meng, E. Hiyama, A. Hosaka, M. Oka, P. Gubler, K. U. Can, T. T. Takahashi, and H. S. Zong, Phys. Lett. B **814**, 136095 (2021).

[23] Q. Qin, Y. F. Shen, and F. S. Yu, Chin. Phys. C **45**, 103106 (2021).

[24] E. Braaten, L. P. He, and A. Mohapatra, Phys. Rev. D **103**, 016001 (2021).

[25] R. Aaij et al. (LHCb Collaboration), arXiv:2109.01038.

[26] R. Aaij et al. (LHCb Collaboration), arXiv:2109.01056.

[27] N. Li, Z. F. Sun, X. Liu, and S. L. Zhu, Phys. Rev. D **88**, 114008 (2013).

[28] L. Meng, G. J. Wang, B. Wang, and S. L. Zhu, Phys. Rev. D **104**, L051502 (2021).

[29] S. K. Choi et al. (Belle Collaboration), Phys. Rev. Lett. **91**, 262001 (2003).

[30] A. Feijoo, W. H. Liang, and E. Oset, Phys. Rev. D **104**, 114015 (2021).

[31] M. J. Yan and M. P. Valderrama, Phys. Rev. D **105**, 014007 (2022).

[32] S. Fleming, R. Hodges, and T. Mehen, Phys. Rev. D **104**, 116010 (2021).

[33] N. Li, Z. F. Sun, X. Liu, and S. L. Zhu, Chin. Phys. Lett. **38**, 092001 (2021).

[34] T. W. Wu, Y. W. Pan, M. Z. Liu, S. Q. Luo, X. Liu, and L. S. Geng, arXiv:2108.00923.

[35] X. Z. Ling, M. Z. Liu, L. S. Geng, E. Wang, and J. J. Xie, Phys. Lett. B **826**, 136897 (2022).

[36] R. Chen, Q. Huang, X. Liu, and S. L. Zhu, Phys. Rev. D **104**, 114042 (2021).

[37] L. Y. Dai, X. Sun, X. W. Kang, A. P. Szczepaniak, and J. S. Yu, arXiv:2108.06002.

[38] X. Z. Weng, W. Z. Deng, and S. L. Zhu, Chin. Phys. C **46**, 013102 (2022).

[39] Q. Xin and Z. G. Wang, arXiv:2108.12597.

[40] Q. Meng, E. Hiyama, A. Hosaka, and M. Oka, Phys. Lett. B **824**, 136800 (2022).

[41] R. Chen, N. Li, Z. F. Sun, X. Liu, and S. L. Zhu, Phys. Lett. B **822**, 136693 (2021).

[42] Y. Huang, H. Q. Zhu, L. S. Geng, and R. Wang, Phys. Rev. D **104**, 116008 (2021).

[43] H. Ren, F. Wu, and R. Zhu, arXiv:2109.02531.

[44] Y. Jin, S. Y. Li, Y. R. Liu, Q. Qin, Z. G. Si, and F. S. Yu, Phys. Rev. D **104**, 114009 (2021).

[45] Y. Hu, J. Liao, E. Wang, Q. Wang, H. Xing, and H. Zhang, Phys. Rev. D **104**, L111502 (2021).

[46] M. Albaladejo, arXiv:2110.02944.

[47] M. Karliner and J. L. Rosner, Phys. Rev. D **105**, 034020 (2022).

[48] L. R. Dai, R. Molina, and E. Oset, Phys. Rev. D **105**, 016029 (2022).

[49] M. Padmanath and N. Mathur, arXiv:2111.01147.

[50] F. L. Wang, R. Chen, and X. Liu, arXiv:2111.00208.

[51] R. Chen, N. Li, Z. F. Sun, X. Liu, and S. L. Zhu, Phys. Lett. B **822**, 136693 (2021).

[52] X. K. Dong, F. K. Guo, and B. S. Zou, Commun. Theor. Phys. **73**, 125201 (2021).

[53] T. W. Wu, Y. W. Pan, M. Z. Liu, S. Q. Luo, L. S. Geng, and X. Liu, Phys. Rev. D **105**, L031505 (2022).

[54] A. Manohar and H. Georgi, Nucl. Phys. **B234**, 189 (1984).

[55] J. Vijande, F. Fernandez, and A. Valcarce, J. Phys. G **31**, 481 (2005).

[56] M. D. Scadron, Phys. Rev. D **26**, 239 (1982).

[57] R. K. Bhaduri, L. E. Cohler, and Y. Nogami, Phys. Rev. Lett. **44**, 1369 (1980).

[58] J. Weinstein and N. Isgur, Phys. Rev. D **27**, 588 (1983).

[59] G. M. Prosperi, M. Raciti, and C. Simolo, Prog. Part. Nucl. Phys. **58**, 387 (2007).

[60] F. Wang, G. H. Wu, L. J. Teng, and T. Goldman, Phys. Rev. Lett. **69**, 2901 (1992); F. Wang, J. L. Ping, G. H. Wu, L. J. Teng, and T. Goldman, Phys. Rev. C **51**, 3411 (1995).

[61] H. X. Huang, J. L. Ping, and F. Wang, Phys. Rev. C **101**, 015204 (2020); H. X. Huang, C. R. Deng, J. L. Ping, and F. Wang, Eur. Phys. J. C **76**, 624 (2016); J. L. Ping, H. R. Pang, F. Wang, and T. Goldman, Phys. Rev. C **65**, 044003 (2002); J. L. Ping, F. Wang, and T. Goldman, Nucl. Phys. **A657**, 95 (1999).

[62] X. Y. Chen and Y. C. Yang, arXiv:2109.02828.

[63] E. Hiyama, Y. Kino, and M. Kamimura, Prog. Part. Nucl. Phys. **51**, 223 (2003).

[64] P. Bicudo, A. Peters, S. Velten, and M. Wagner, Phys. Rev. D **103**, 114506 (2021).

[65] A. Francis, R. J. Hudspith, R. Lewis, and K. Maltman, Phys. Rev. Lett. **118**, 142001 (2017).

[66] P. Junnarkar, N. Mathur, and M. Padmanath, Phys. Rev. D **99**, 034507 (2019).

[67] M. Wagner, P. Bicudo, A. Peters, and S. Velten, arXiv:2108.11731.

[68] Y.-R. Liu, H.-X. Chen, W. Chen, X. Liu, and S.-L. Zhu, Prog. Part. Nucl. Phys. **107**, 237 (2019).

[69] L. Maiani, A. D. Polosa, and V. Riquer, Phys. Rev. D **100**, 074002 (2019).

[70] J. M. Richard, A. Valcarce, and J. Vijande, arXiv:2112.04300.

[71] T. F. Caramés, J. Vijande, and A. Valcarce, Phys. Rev. D **99**, 014006 (2019).

[72] M. Pflaumer, L. Leskovec, S. Meinel, and M. Wagner, arXiv:2108.10704.

[73] R. J. Hudspith, B. Colquhoun, A. Francis, R. Lewis, and K. Maltman, Phys. Rev. D **102**, 114506 (2020).

[74] G. Yang, J. L. Ping, and J. Segovia, Phys. Rev. D **102**, 054023 (2020).

[75] Y. H. Wu, X. Jin, R. X. Liu, H. X. Huang, and J. L. Ping, arXiv:2112.05967.

[76] K. Azizi and U. Özdem, Phys. Rev. D **104**, 114002 (2021).

[77] L. Y. Glozman and A. V. Nefediev, Nucl. Phys. **A807**, 38 (2008).